IEEE Access
Multidisciplinary ⋮ Rapid Review ⋮ Open Access Journal

Received August 16, 2020, accepted September 2, 2020, date of publication September 7, 2020,
date of current version September 18, 2020.

Digital Object Identifier 10.1109/ACCESS.2020.3022097

A Spatially Adaptive Edge-Preserving Denoising Method Based on Fractional-Order Variational PDEs

DEHUA WANG[1,2], JUAN J. NIETO[3], XIAOPING LI[2], AND YIMING LI[4]

[1]School of Sciences, Xi'an Technological University, Xi'an 710021, China
[2]School of Mathematical Sciences, University of Electronic Science and Technology of China, Chengdu 610054, China
[3]Departamento de Estatística, Análisis Matemático e Optimización, Instituto de Matemáticas, Universidade de Santiago de Compostela, 15782 Santiago de Compostela, Spain
[4]Department of Mathematical Sciences, Fudan University, Shanghai 200433, China

Corresponding author: Xiaoping Li (lixiaoping.math@uestc.edu.cn)

The work of Dehua Wang was supported in part by the Science and Technology Planning Project of Shaanxi Province under Grant 2020JM-561, in part by the Postdoctoral Foundation of China under Grant 2019M663462, in part by the Innovative Talents Cultivate Program of Shaanxi Province under Grant 2019KJXX-032, in part by the President Fund of Xi'an Technological University under Grant XAGDXJJ17026, and in part by the Teaching Reform Project of Xi'an Technological University under Grant 18JGY08. The work of Juan J. Nieto was supported in part by the Agencia Estatal de Investigacion (AEI) of Spain under Grant MTM2016-75140-P, and in part by the European Community Fund FEDER. The work of Xiaoping Li was supported in part by the NSFC under Grant 61701086, and in part by the Fundamental Research Funds for the Central Universities under Grant ZYGX2016KYQD143.

ABSTRACT Image denoising is a basic problem in image processing. An important task of image denoising is to preserve the significant geometric features such as edges and textures while filtering out noise. So far, this is still a problem to be further studied. In this paper, we firstly introduce an edge detection function based on the Gaussian filtering operator and then analyze the filtering characteristic of the fractional derivative operator. On the basis, we establish the spatially adaptive fractional edge-preserving denoising model in the variational framework, discuss the existence and uniqueness of our proposed model solution and derive the nonlinear fractional Euler-Lagrange equation for solving our proposed model. This forms a fractional order extension of the first and second order variational approaches. Finally, we apply the proposed method to the synthetic images and real seismic data denoising to verify the effectiveness of our method and compare the experimental results of our method with the related state-of-the-art methods. Experimental results illustrate that our proposed method can not only improve the signal to noise ratio (SNR) but also adaptively preserve the structural information of an image compared with other contrastive methods. Our proposed method can also be applied to remote sensing imaging, medical imaging and so on.

INDEX TERMS Calculus of variations, fractional-order derivative, nonlinear partial differential equations, denoising, edge-preserving.

I. INTRODUCTION

Image denoising is an important issue in information processing field. In the last decade, many popular methods, including partial differential equation (PDE) based methods [1]–[3], dictionary learning [4], [5], sparse representation [5]–[7] and non-negative matrix factorization based methods [8] etc., emerge in these fields such as signal and image processing, medical, seismic and remote sensing imaging and compressed sensing. In this paper, we mainly focus on the PDE-based image denoising methods. The studies on this issue are primarily based on nonlinear diffusion [9]–[13], or the minimization of energy functional in the variational framework [14]–[22]. In this work, we focus on the latter.

Among the variational methods, the pathbreaking work is the total variation (TV) based noise removal model proposed in [14] by Rudin, Osher and Fatemi. The TV model can be written as

$$\min_u \int_\Omega |\nabla u| dxdy + \frac{\lambda}{2}\int_\Omega (u-u_0)^2 dxdy. \tag{1}$$

In this model, $u_0(x, y)$ and $u(x, y)$ respectively denote the observed noisy image and the denoised image at $x, y \in \Omega$,

The associate editor coordinating the review of this manuscript and approving it for publication was Larbi Boubchir.

∇u denotes the gradient of $u(x, y)$ with $|\nabla u| = \sqrt{u_x^2 + u_y^2}$ and $\lambda > 0$ is a parameter. An anisotropic version of the TV based algorithm [23] is described as

$$\min_u \int_\Omega (|u_x| + |u_y|)dxdy + \frac{\lambda}{2}\int_\Omega (u - u_0)^2 dxdy. \quad (2)$$

The most noteworthy feature of the TV based algorithm is that it can successfully preserve the sharp edges in images [24]. Unsatisfactorily, in [25], the authors have shown that the minimization of TV norm often results in a piecewise constant image. The so-called staircase effect often leads to false edges which do not exist in the true image.

To overcome this false staircase effect caused by the minimization of TV norm, higher order derivatives were introduced and the high-order PDE based denoising models have largely alleviated the staircase effect [26]–[30]. The denoising model based on the high-order PDE was first proposed in [28] by Lysaker, Lundervold and Tai (LLT). The LLT model can be described as

$$\min_u \int_\Omega (|u_{xx}| + |u_{yy}|)dxdy + \frac{\lambda}{2}\int_\Omega (u - u_0)^2 dxdy. \quad (3)$$

Unfortunately, it seems to be difficult to preserve discontinuities in an image while filtering noise [31]. In the [32], Bredies *et al.* introduced a regularization functional named total generalized variation (TGV) defined by

$$\mathrm{TGV}_\alpha^k(u) = \sup\left\{ \int_\Omega u \,\mathrm{div}^k v \mathrm{d}x | v \in \mathcal{C}_c^k(\Omega, \mathrm{Sym}^k(\mathbb{R}^d)), \right.$$
$$\left. \|\mathrm{div}^l v\|_\infty \le \alpha_l, l = 0, \ldots, k-1 \right\} \quad (4)$$

where $\mathrm{Sym}^k\left(\mathbb{R}^d\right)$ denotes the space of symmetric tensors of order $k \ge 2$ with arguments in $\mathbb{R}^d$, $\mathcal{C}_c^k\left(\Omega, \mathrm{Sym}^k\left(\mathbb{R}^d\right)\right)$ denotes the compactly supported vector space of k times continuously differentiable $\mathrm{Sym}^k\left(\mathbb{R}^d\right)$-valued mappings, and $\alpha_0, \ldots, \alpha_{k-1}$ are fixed positive parameters. It can effectively overcome the undesired staircase artifacts and achieved an optimal tradeoff between the first and second derivative. However, the TGV is not allowed to measure the directional information of noisy data because of its rotation invariance.

Recently, Zhang and Wei in [33], [34] thought that the fractional-order derivative filtering can alleviate the staircase effect and preserve the textures and details while denoising. They replaced the integer order derivative in TV regularization term with the fractional order derivative and then proposed the following fractional total variation (FTV) denoising model

$$\min_u \int_\Omega |\nabla^\alpha u| dxdy + \frac{\lambda}{2}\int_\Omega (u - u_0)^2 dxdy. \quad (5)$$

where $|\nabla^\alpha u| := \sqrt{(D_x^\alpha u)^2 + (D_y^\alpha u)^2}$, $D_x^\alpha u$ and $D_y^\alpha u$ respectively denote the α-order derivatives of u with respect to the variables x and y. The latest published works on the use of fractional-order total variation are referred to the [35]–[41]. It is worth noting that the orders of fractional derivatives in these works are all constant.

In fact, the use of constant-order fractional derivatives may not be the best option, since there are different characteristics in different image regions, and the fractional derivatives of different orders need to be used while processing different regions. In 2014, Wang and Gao in [42] proposed a denoising method based on anisotropic fractional-gradient operators as follows

$$\min_u \int_\Omega \left|\nabla^{(\alpha_1,\alpha_2)} u\right| \mathrm{d}x\mathrm{d}y + \frac{\lambda}{2}\int_\Omega (u - u_0)^2 dxdy, \quad (6)$$

where u_0 denotes the noisy image, u is the denoised image, α_1, α_2 denote the orders of fractional derivative in the horizontal and vertical directions respectively, $\left|\nabla^{(\alpha_1,\alpha_2)} u\right| := \sqrt{(D_x^{\alpha_1} u)^2 + (D_y^{\alpha_2} u)^2}$ which can meet different filtering requirements in different directions, and $\lambda > 0$ is a regularization parameter. This method only consider the horizontal and vertical directions of noisy data. In fact, most directional information in natural images are often spatially varying. Therefore, it is meaningful to generalize the order of derivative to be a function depending on spatial variables.

In this paper, we employ the variable-order fractional derivative to replace the one of constant order in equation (5), and establish a spatially adaptive fractional variational denoising model. The motivation of this work is to develop a new method which can not only effectively filter noise but also adaptively preserve important structural information such as edges. The contribution lies in (i) introducing an edge detection function based on Gaussian filtering operator; (ii) establishing the spatially adaptive fractional edge-preserving denoising model in the variational framework; (iii) discussing the existence and uniqueness of the solution of our proposed model; (iv) presenting the selection strategy of regularization parameter and iteration number.

The rest of this paper is organized as follows. In Section 2, we introduce an edge detection function based on nonlinear diffusion. In Section 3, we first analyze the filtering characteristic of the fractional derivative operator, and then establish the spatially adaptive fractional edge-preserving denoising model in the variational framework, Furthermore, we discuss the existence and uniqueness of the solution of our proposed model. Finally, we derive the nonlinear fractional PDE for solving the proposed model. In Section 4, we give the numerical implementation scheme for solving the nonlinear PDE. Section 5 demonstrates the performance of our proposed method via comparative experiments for the synthetic images and noisy real seismic data. Some conclusions are presented in Section 6.

II. THE CHARACTERIZATION OF EDGE FEATURES

Edge detection by nonlinear diffusion first appeared in the early work of Perona and Malik [9]. They considered the nonlinear PDE

$$\frac{\partial u}{\partial t} = \mathrm{div}\big(g(|\nabla u|)\nabla u\big), \quad u|_{t=0} = u_0. \quad (7)$$

In above equation, u_0 denotes an initial noisy image, g is a nonincreasing smooth function with $g(0) = 1$, $g(x) \ge 0$, and

$g(x)$ tending to zero at infinity. The main idea is to reduce the smoothness in the presence of edges. It follows that the edge detector can be described as

$$e_1(x,y) := g(|\nabla u_0|) = \frac{1}{1+k|\nabla u_0|^2}. \tag{8}$$

However, an obvious drawback of this edge detector is that it is not well suitable for the case in the presence of noise. Later, Catté *et al.* in [43] replaced the gradient $|\nabla u|$ in (7) by its Gaussian smoothing version and the equation (7) is modified as

$$\frac{\partial u}{\partial t} = \operatorname{div}\left(g\left(|\nabla(G_\sigma * u)|\right)\nabla u\right), \quad u|_{t=0} = u_0. \tag{9}$$

Here, the edge detector can be described as

$$\begin{aligned} e_2(x,y) &:= g(|\nabla(G_\sigma * u_0)|) \\ &= \frac{1}{1+k|\nabla(G_\sigma * u_0)|^2}, \quad k>0, \sigma>0 \end{aligned} \tag{10}$$

where G_σ denotes a two-dimensional Gaussian filter with the standard deviation σ and $G_\sigma * u_0$ denotes a filtering version of u_0 which is independent of the time variable. The edge detector is immune to the influence of the noise when detecting the edges in a noisy image. We note that the bigger the parameter σ, the wider the obtained edges [44]. In next section, we will employ the edge detector $e_2(x,y)$ to define the spatially variable order of the fractional derivative.

III. METHOD

In this section, we first analyze the filtering characteristic of the fractional derivative operator. Next, we formulate a variational PDE based denoising model and present the existence and uniqueness conclusions of its solution. Finally, we derive the nonlinear fractional PDE for solving the proposed model.

A. THE FILTERING CHARACTERISTICS OF THE FRACTIONAL DIFFERENTIAL OPERATOR

The frequency response of a fractional differential operator can be considered as a nonlinear filter [33]. Its amplitude-frequency response characteristics are shown in Figure 1, which shows that the fractional differential operators are approximately high-pass filters as $\alpha > 0$. That is to say, high-frequency components of a signal can be nonlinearly enhanced and its low-frequency components are suppressed [45]. As seen in Figure 1, the high-pass ability becomes stronger as α increases. Thus, when $0 < \alpha < 1$, the high-pass ability is weaker than the case of $\alpha \geq 1$, which leads to some useful high-frequency information, like edges etc., may also be filtered together with the high-frequency noise. On the contrary, if α is too large, the ability to enhance high-frequency components is too strong to effectively remove the high-frequency noise. Therefore, α is chosen between 1 and 2 in order to preserve the useful high-frequency information while effectively suppressing the high-frequency noise.

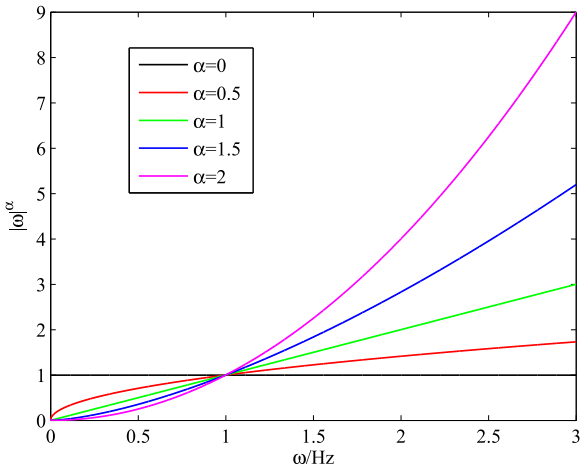

FIGURE 1. The amplitude-frequency response curves of fractional differential operators with different orders.

B. DESCRIPTION OF THE PROPOSED MODEL

Based on the edge detection function (10) in Section II and the filtering characteristic of the fractional derivative in Section III-A, we define the variable-order $\alpha(x,y)$ of the fractional derivative as follows

$$\alpha(x,y) := 1 + \frac{1}{1+k|\nabla(G_\sigma * u_0)|^2}, \tag{11}$$

where u_0 denotes the observed data, $\sigma > 0$ is the standard deviation of Gaussian filter G_σ and $k > 0$ is a parameter which depends on the noise level of noisy data.

The proposed variational model is described as the following minimization problem of energy functional

$$\min_u \left\{ E(u) := J^{\alpha(x,y)}(u) + \frac{\lambda}{2}H(u) \right\}. \tag{12}$$

In this model, u is defined in the space of variable-order fractional bounded variation functions

$$BV^{\alpha(x,y)}(\Omega) := \left\{ u \in L^1(\Omega) \mid J^{\alpha(x,y)}(u) < +\infty \right\} \tag{13}$$

with the norm

$$\|u\|_{BV^{\alpha(x,y)}} = \|u\|_{L^1} + J^{\alpha(x,y)}(u), \tag{14}$$

$J^{\alpha(x,y)}(u)$ is defined as

$$J^{\alpha(x,y)}(u) := \int_\Omega |\nabla^{\alpha(x,y)} u| dxdy \tag{15}$$

with

$$\nabla^{\alpha(x,y)} u := \left({}_{a_1}D_x^{\alpha(x,y)} u, {}_{a_2}D_y^{\alpha(x,y)} u \right)$$

and

$$|\nabla^{\alpha(x,y)} u| := \int_\Omega \sqrt{\left({}_{a_1}D_x^{\alpha(x,y)} u\right)^2 + \left({}_{a_2}D_y^{\alpha(x,y)} u\right)^2} dxdy,$$

and $H(u) = \int_\Omega (u-u_0)^2 dxdy$ is defined in the $L^2(\Omega)$ and $E(u)$ is defined in $BV^{\alpha(x,y)}(\Omega) \cap L^2(\Omega)$. On the parts of an

image where edges are present, $|\nabla(G_\sigma * u_0)|$ is very large and $\alpha(x, y)$ tends to 1, in which case our proposed model is approximate to the TV model; on the homogeneous regions, $|\nabla(G_\sigma * u_0)|$ is very small and $\alpha(x, y)$ tends to 2, in which case our proposed model is approximate to the LLT model. Therefore, our proposed model can theoretically preserve the edge information while filtering out noise. About this model, we give some more detailed notes as follows:

(i) $\Omega \subset \mathbb{R}^2$ is the domain where an image is defined, u_0 and u respectively denote an initial noisy image and the denoised image and $\lambda > 0$ is a parameter;

(ii) According to the [46], the variable-order fractional derivatives of $u(x, y)$ at a point (x, y) with respect to the variables x and y are defined as given in (16) and (17), as shown at the bottom of the page, where $\binom{\alpha(x,y)}{k} = \frac{\Gamma(\alpha(x,y)+1)}{\Gamma(k+1)\Gamma(\alpha(x,y)-k+1)}$ and $\Gamma(x) = \int_0^\infty e^{-t}t^{x-1}\mathrm{d}t$.

(iii) our proposed method is suitable for removing the random noise in two dimensional data due to the fact that L^2 norm is used to measure the random noise.

Next, we establish the existence and uniqueness theories of the solution of the proposed model (12). The theories follow from the next lemmas.

Lemma 1 (Lower Semi-Continuity): Let $\{u_n(x, y)\}$ be a function sequence in $BV^{\alpha(x,y)}(\Omega)$ converging in $L^1(\Omega)$ to a function $u(x, y)$. Then $\liminf_{n\to\infty} J^{\alpha(x,y)}(u_n) \geq J^{\alpha(x,y)}(u)$.

Proof 1: Since all the functions $u_n(x, y)$ of the sequence and their limit function $u(x, y)$ are integrable, by Fatou's lemma [47],

$$\begin{aligned}\liminf_{n\to\infty}\int_\Omega |\nabla^{\alpha(x,y)}u_n|dxdy &\geq \int_\Omega \liminf_{n\to\infty}|\nabla^{\alpha(x,y)}u_n|dxdy\\ &= \int_\Omega |\nabla^{\alpha(x,y)}\lim_{n\to\infty}u_n|dxdy = \int_\Omega |\nabla^{\alpha(x,y)}u|dxdy.\end{aligned}$$

Thus $\liminf_{n\to\infty} J^{\alpha(x,y)}(u_n) \geq J^{\alpha(x,y)}(u)$ holds. The inequality shows that $J^{\alpha(x,y)}(u)$ is lower semi-continuous.

Lemma 2: The space $BV^{\alpha(x,y)}(\Omega)$ is a Banach space.

Proof 2: Based on the definitions of $BV^{\alpha(x,y)}(\Omega)$ and $\|u\|_{BV^{\alpha(x,y)}}$, we can easily verify that the space $BV^{\alpha(x,y)}(\Omega)$ is a normed space. So it only needs to prove the completeness.

Suppose $\{u_n\}$ is a Cauchy sequence in $BV^{\alpha(x,y)}(\Omega)$, then it is also a Cauchy sequence in $L^1(\Omega)$. Since the space $L^1(\Omega)$ is complete, there exists a function $u \in L^1(\Omega)$ such that $u_n \to u$. Since the Cauchy sequence $\{u_n\}$ in $BV^{\alpha(x,y)}(\Omega)$ is bounded for each n, then $\|u_n\|_{BV^{\alpha(x,y)}} < +\infty$ and thus $J^{\alpha(x,y)}(u_n) < +\infty$ by the definition of $\|\cdot\|_{BV^{\alpha(x,y)}}$. According to Lemma 1, we have $J^{\alpha(x,y)}(u) < +\infty$. We have showed that $u \in BV^{\alpha(x,y)}(\Omega)$. Finally, we shall prove that $u_n \to u$ in $BV^{\alpha(x,y)}(\Omega)$. Again by Lemma 1, for an arbitrary small positive number ϵ,

$$\begin{aligned}&\|u_n - u_m\|_{BV^{\alpha(x,y)}(\Omega)} < \epsilon \ \ \forall n, m \geq N \in \mathbb{N}\\ &\qquad \Rightarrow J^{\alpha(x,y)}(u_n - u) \leq \liminf_{m\to\infty} J^{\alpha(x,y)}(u_n - u_m) \leq \epsilon,\end{aligned}$$

which shows that $u_n \to u$ in $BV^{\alpha(x,y)}(\Omega)$. It follows that $BV^{\alpha(x,y)}(\Omega)$ is a Banach space.

Lemma 3: The functional $E(u)$ is coercive on $BV^{\alpha(x,y)}(\Omega) \cap L^2(\Omega)$.

$$\begin{cases} {}_{a_1}D_x^{\alpha(x,y)}u(x,y) = \lim\limits_{\substack{h\to 0\\ nh=x-a_1}} h^{-\alpha(x,y)}\sum\limits_{k=0}^{n}(-1)^k\binom{\alpha(x,y)}{k}u(x-kh,y), & \text{(left-sided)}\\ {}_{x}D_{b_1}^{\alpha(x,y)}u(x,y) = \lim\limits_{\substack{h\to 0\\ nh=b_1-x}} h^{-\alpha(x,y)}\sum\limits_{k=0}^{n}(-1)^k\binom{\alpha(x,y)}{k}u(x+kh,y), & \text{(right-sided)}\end{cases} \tag{16}$$

and

$$\begin{cases} {}_{a_2}D_y^{\alpha(x,y)}u(x,y) = \lim\limits_{\substack{h\to 0\\ nh=y-a_2}} h^{-\alpha(x,y)}\sum\limits_{k=0}^{n}(-1)^k\binom{\alpha(x,y)}{k}u(x,y-kh), & \text{(left-sided)}\\ {}_{y}D_{b_2}^{\alpha(x,y)}u(x,y) = \lim\limits_{\substack{h\to 0\\ nh=b_2-y}} h^{-\alpha(x,y)}\sum\limits_{k=0}^{n}(-1)^k\binom{\alpha(x,y)}{k}u(x,y+kh), & \text{(right-sided)}\end{cases} \tag{17}$$

$$\begin{aligned}&J^{\alpha(x,y)}\big(tu+(1-t)v\big)\\ &= \int_\Omega \sqrt{\Big({}_{a_1}D_x^{\alpha(x,y)}\big(tu+(1-t)v\big)\Big)^2 + \Big({}_{a_2}D_y^{\alpha(x,y)}\big(tu+(1-t)v\big)\Big)^2}dxdy\\ &= \int_\Omega \sqrt{\big(t\,{}_{a_1}D_x^{\alpha(x,y)}u + (1-t)\,{}_{a_1}D_x^{\alpha(x,y)}v\big)^2 + \big(t\,{}_{a_1}D_y^{\alpha(x,y)}u + (1-t)\,{}_{a_1}D_y^{\alpha(x,y)}v\big)^2}dxdy\\ &\leq \int_\Omega \Big(t\sqrt{\big({}_{a_1}D_x^{\alpha(x,y)}u\big)^2 + \big({}_{a_1}D_y^{\alpha(x,y)}u\big)^2} + (1-t)\sqrt{\big({}_{a_1}D_x^{\alpha(x,y)}v\big)^2 + \big({}_{a_1}D_y^{\alpha(x,y)}v\big)^2}\Big)dxdy\\ &= t\int_\Omega \sqrt{\big({}_{a_1}D_x^{\alpha(x,y)}u\big)^2 + \big({}_{a_1}D_y^{\alpha(x,y)}u\big)^2}dxdy + (1-t)\int_\Omega \sqrt{\big({}_{a_1}D_x^{\alpha(x,y)}v\big)^2 + \big({}_{a_1}D_y^{\alpha(x,y)}v\big)^2}dxdy\\ &= tJ^{\alpha(x,y)}(u) + (1-t)J^{\alpha(x,y)}(v).\end{aligned} \tag{18}$$

Proof 3: Since $\lambda > 0$ and $H(u) \geq 0$, for any sequence $\{u_k\} \subset BV^{\alpha(x,y)}(\Omega)$, we have $E(u_k) \geq J^{\alpha(x,y)}(u_k) \to \infty$ as $\|u_k\|_{BV^{\alpha(x,y)}} \to \infty$ according to the definition of $\|\cdot\|_{BV^{\alpha(x,y)}}$. So $E(u)$ is coercive on $BV^{\alpha(x,y)}(\Omega)$. For any sequence $\{u_k\} \subset L^2(\Omega)$, we have $E(u_k) \geq \frac{\lambda}{2}H(u_k) = \frac{\lambda}{2}\|u_k - u_0\|_2^2 \geq (\|u_k\|_2 - \|u_0\|_2)^2 \to \infty$ as $\|u_k\|_2 \to \infty$, thus $E(u)$ is also coercive on $L^2(\Omega)$. Therefore, $E(u)$ is coercive on $BV^{\alpha(x,y)}(\Omega) \cap L^2(\Omega)$.

Lemma 4: The functional $J^{\alpha(x,y)}(u)$ is convex.

Proof 4: It is easy to verify that $BV^{\alpha(x,y)}(\Omega)$ is a non-empty convex set. For any $u, v \in BV^{\alpha(x,y)}(\Omega), t \in (0,1)$, we have that the result as given in (18), as shown at the bottom of the previous page. The convexity of $J^{\alpha(x,y)}(u)$ is proved.

Applying the above lemmas to problem (12), we can obtain the following theorem.

Theorem 1 (The Existence and Uniqueness): The functional $E(u)$ has a unique minimizer in $BV^{\alpha(x,y)}(\Omega) \cap L^2(\Omega)$.

Proof 5: We first prove the existence. By Lemma 2, $BV^{\alpha(x,y)}(\Omega)$ is a Banach space. Also, $L^2(\Omega)$ is a Hilbert space. It follows from the completeness of the both spaces that $BV^{\alpha(x,y)}(\Omega) \cap L^2(\Omega)$ is a Banach space. According to Lemma 1, $J^{\alpha(x,y)}(u)$ is lower semi-continuous on $BV^{\alpha(x,y)}(\Omega)$. Also, the lower semi-continuity of $H(u)$ on $L^2(\Omega)$ also holds as proven in [48]. It follows that $E(u)$ is lower semi-continuous on $BV^{\alpha(x,y)}(\Omega) \cap L^2(\Omega)$. The coercivity of $E(u)$ has been proved by Lemma 3. Thus, there exists a minimizer such that the functional $E(u)$ attains a minimum on $BV^{\alpha(x)}(\Omega) \cap L^2(\Omega)$. Then we prove the uniqueness. Since $J^{\alpha(x)}(u)$ is a convex functional on $BV^{\alpha(x,y)}(\Omega)$ (see Lemma 4) and $H(u)$ is a strictly convex functional on $L^2(\Omega)$, $E(u)$ is a convex functional on $BV^{\alpha(x,y)}(\Omega) \cap L^2(\Omega)$. The convexity of $E(u)$ guarantees the uniqueness of the minimizer. Therefore, the functional $E(u)$ has a unique minimizer in $BV^{\alpha(x,y)}(\Omega) \cap L^2(\Omega)$.

Finally, we derive a fractional Euler-Lagrange equation for solving the proposed variational model. Take any test function $\eta(x,y) \in C^1(\Omega)$ such that ${}_{a_1}D_x^{\alpha(x,y)}\eta, {}_{a_2}D_y^{\alpha(x,y)}\eta \in C(\Omega)$. For arbitrary $\epsilon > 0$ and $|a| < \epsilon$, we define

$$\begin{aligned}\Phi(a) &:= E(u + a\eta) \\ &= \int_\Omega \sqrt{\left({}_{a_1}D_x^{\alpha(x,y)}(u + a\eta)\right)^2 + \left({}_{a_2}D_y^{\alpha(x,y)}(u + a\eta)\right)^2} \\ &\quad + \frac{\lambda}{2}(u + a\eta - u_0)^2 dxdy. \end{aligned} \tag{19}$$

So, it has the following equation (20), as shown at the bottom of the page. Thus, we can obtain that the value of $\Phi'(a)$ as $a = 0$ equals the equation (21), as shown at the bottom of the page, where $\left({}_{a_1}D_x^{\alpha(x,y)}\right)^*$ and $\left({}_{a_2}D_y^{\alpha(x,y)}\right)^*$ are the adjoint operators of ${}_{a_1}D_x^{\alpha(x,y)}$ and ${}_{a_2}D_y^{\alpha(x,y)}$ respectively.

Let $\Phi'(0) = 0$, then u satisfies the following fractional Euler-Lagrange equation

$$\begin{aligned}\left({}_{a_1}D_x^{\alpha(x,y)}\right)^* \frac{{}_{a_1}D_x^{\alpha(x,y)}u}{|\nabla^{\alpha(x,y)}u|} + \left({}_{a_2}D_y^{\alpha(x,y)}\right)^* \frac{{}_{a_2}D_y^{\alpha(x,y)}u}{|\nabla^{\alpha(x,y)}u|} \\ +\lambda(u - u_0) = 0. \end{aligned} \tag{22}$$

By introducing an artificial time parameter, this PDE can be solved through the following steepest descent procedure

$$\begin{aligned}\frac{\partial u}{\partial t} = -\left({}_{a_1}D_x^{\alpha(x,y)}\right)^* \frac{{}_{a_1}D_x^{\alpha(x,y)}u}{|\nabla^{\alpha(x,y)}u|} - \left({}_{a_2}D_y^{\alpha(x,y)}\right)^* \frac{{}_{a_2}D_y^{\alpha(x,y)}u}{|\nabla^{\alpha(x,y)}u|} \\ -\lambda(u - u_0). \end{aligned} \tag{23}$$

IV. NUMERICAL IMPLEMENTATION

In this section, we employ the semi-implicit gradient descent scheme for solving the nonlinear PDE (23). Assume that the involved image can be expressed as a matrix with size of $N \times N$. We denote the time step size as Δt and the space grid size as h, and so the time and space can be discretized as

$$t = n\Delta t, \quad x = ih, \ y = jh,$$

where $n = 0, 1, 2, \ldots, i, j = 1, 2, \ldots, N$. The discrete scheme of the nonlinear PDE (23) is expressed as

$$\begin{aligned}u_{i,j}^{n+1} = u_{i,j}^n + \Delta t\Bigg(&- \left(\left({}_{a_1}D_x^{\alpha(x,y)}\right)^* \frac{{}_{a_1}D_x^{\alpha(x,y)}u^n}{|\nabla^{\alpha(x,y)}u^n|}\right)_{i,j} \\ &- \left(\left({}_{a_2}D_y^{\alpha(x,y)}\right)^* \frac{{}_{a_2}D_y^{\alpha(x,y)}u^n}{|\nabla^{\alpha(x,y)}u^n|}\right)_{i,j} - \lambda(u_{i,j}^n - u_{i,j}^0)\Bigg) \end{aligned} \tag{24}$$

with the initial condition $u_{i,j}^0 = u_0(ih, jh)$ for $i, j = 1, 2, \ldots, N$.

In equation (24), $\left({}_{a_1}D_x^{\alpha(x,y)}u^n\right)_{i,j}$, $\left({}_{a_2}D_y^{\alpha(x,y)}u^n\right)_{i,j}$ can be expressed as

$$\begin{cases}\left({}_{a_1}D_x^{\alpha(x,y)}u^n\right)_{i,j} = \sum_{k=0}^{i-1}(-1)^k \binom{\alpha_{i,j}}{k} u_{i-k,j}, \\ \left({}_{a_2}D_y^{\alpha(x,y)}u^n\right)_{i,j} = \sum_{k=0}^{j-1}(-1)^k \binom{\alpha_{i,j}}{k} u_{i,j-k}. \end{cases} \tag{25}$$

$$\Phi'(a) = \int_\Omega \left(\frac{{}_{a_1}D_x^{\alpha(x,y)}(u + a\eta)\,{}_{a_1}D_x^{\alpha(x,y)}\eta + {}_{a_2}D_y^{\alpha(x,y)}(u + a\eta)\,{}_{a_2}D_y^{\alpha(x,y)}\eta}{\sqrt{\left({}_{a_1}D_x^{\alpha(x,y)}(u + a\eta)\right)^2 + \left({}_{a_2}D_y^{\alpha(x,y)}(u + a\eta)\right)^2}} + \lambda(u + a\eta - u_0)\eta \right) dxdy. \tag{20}$$

$$\begin{aligned}\Phi'(0) &= \int_\Omega \left(\frac{{}_{a_1}D_x^{\alpha(x,y)}u\,{}_{a_1}D_x^{\alpha(x,y)}\eta + {}_{a_2}D_y^{\alpha(x,y)}u\,{}_{a_2}D_y^{\alpha(x,y)}\eta}{\sqrt{\left({}_{a_1}D_x^{\alpha(x,y)}u\right)^2 + \left({}_{a_2}D_y^{\alpha(x,y)}u\right)^2}} + \lambda(u - u_0)\eta \right) dxdy \\ &= \int_\Omega \left(\left({}_{a_1}D_x^{\alpha(x,y)}\right)^* \frac{{}_{a_1}D_x^{\alpha(x,y)}u}{|\nabla^{\alpha(x,y)}u|} + \left({}_{a_2}D_y^{\alpha(x,y)}\right)^* \frac{{}_{a_2}D_y^{\alpha(x,y)}u}{|\nabla^{\alpha(x,y)}u|} + \lambda(u - u_0) \right)\eta dxdy, \end{aligned} \tag{21}$$

One can check that the formulae (26) and (27), as shown at the bottom of the page hold.

Now, we present the numerical algorithm to solve the nonlinear fractional PDE (23) as follows

Algorithm 1 The Semi-Implicit Gradient Descent Scheme

Input: the noisy image u_0, the number of iterations K, k, Δt and λ;

Initialization: $n = 1$, $u_{i,j}^n = u_{i,j}^0$ for $i, j = 1, 2, \ldots, N$;

Compute the value of $\alpha_{i,j}$ according to (11) for $i, j = 1, 2, \ldots, N$;

for $n = 1 : K$ **do**

Compute $\left(\left({}_{a_1}D_x^{\alpha(x,y)}\right)^* \frac{a_1 D_x^{\alpha(x,y)} u^n}{|\nabla^{\alpha(x,y)} u^n|}\right)_{i,j}$ and $\left(\left({}_{a_2}D_y^{\alpha(x,y)}\right)^* \frac{a_2 D_y^{\alpha(x,y)} u^n}{|\nabla^{\alpha(x,y)} u^n|}\right)_{i,j}$ for $i, j = 1, 2, \ldots, N$ according to (16), (17), (26) and (27);

Compute $u_{i,j}^{n+1} = u_{i,j}^n + \Delta t\Big(- (D_x^\alpha)^* \frac{D_x^\alpha u_{i,j}^n}{|D_x^\alpha u_{i,j}^n|} - (D_y^\alpha)^* \frac{D_y^\alpha u_{i,j}^n}{|D_y^\alpha u_{i,j}^n|} - \lambda(u_{i,j}^n - u_{i,j}^0)\Big)$ for $i, j = 1, 2, \ldots, N$;

$n = n + 1$;

end for

Output: the denoised image u^n.

At last, we analyze the computational complexity for Algorithm 1. In this algorithm, the number of iterations K is a fixed value. The main per-iteration cost lies in the update of $\left(\left({}_{a_1}D_x^{\alpha(x,y)}\right)^* \frac{a_1 D_x^{\alpha(x,y)} u^n}{|\nabla^{\alpha(x,y)} u^n|}\right)_{i,j}$ and $\left(\left({}_{a_2}D_y^{\alpha(x,y)}\right)^* \frac{a_2 D_y^{\alpha(x,y)} u^n}{|\nabla^{\alpha(x,y)} u^n|}\right)_{i,j}$ for $i, j = 1, 2, \ldots, N$. In each iteration, according to (27), we need to perform $N + j + 2$ additions and 8 multiplications when we compute $\left(\left({}_{a_1}D_x^{\alpha(x,y)}\right)^* \frac{a_1 D_x^{\alpha(x,y)} u^n}{|\nabla^{\alpha(x,y)} u^n|}\right)_{i,j}$ for each fixed (i, j). Meanwhile, the computation of $\left(\left({}_{a_2}D_y^{\alpha(x,y)}\right)^* \frac{a_2 D_y^{\alpha(x,y)} u^n}{|\nabla^{\alpha(x,y)} u^n|}\right)_{i,j}$ also possesses similar complexity with $\left(\left({}_{a_1}D_x^{\alpha(x,y)}\right)^* \frac{a_1 D_x^{\alpha(x,y)} u^n}{|\nabla^{\alpha(x,y)} u^n|}\right)_{i,j}$. So, in Algorithm 1, K iterations will totally need to perform about $KN^2(2N + i + j + 4)$ additions and $16KN^2$ multiplications.

V. EXPERIMENTAL RESULTS

In this section, we apply the proposed method to the synthetic images and real seismic data denoising to verify the effectiveness of our method. We choose the rectangular region I to verify the effectiveness of our method for processing the smooth region of an image, choose the rectangular region II and the test image IV to verify the ability to preserve the edges in noisy images while denoising, choose the test image III to verify the ability to preserve the structural information and choose the test image V to verity the ability to preserve the detailed information while denoising. Furthermore, the real seismic data is used in experiments to prove that our proposed method is well suitable for processing the real noisy data.

A. SYNTHETIC IMAGE EXPERIMENTS

In this subsection, we first use the standard test image as shown in Fig. 4(a) to present the choice scheme of parameters involved in this test, and then compare the proposed method with the related methods like TV, LLT, TGV, FTV and structure-oriented directional total generalized variation (SODTGV) denoising method [49] in different noise standard deviations $\sigma = 10$, $\sigma = 20$, $\sigma = 30$.

In order to get a meaningful solution of problem (12), it is necessary to estimate the optimal value of the regularization parameter λ. L-curve method is a usual approach for the optimal selection of the regularization parameter. This curve which is a log-log plot between the norm of the regularized solution and the residual norm appears a typical "L" shape, and the optimal value of λ is considered to be the corner of the "L". Here, we plot the L-curve of problem (12) for the noisy image u_0 with the standard deviation of noise $\sigma = 20$ as shown in Figure 2. It's clear that $\lambda = 0.01$ is the optimal selection in the values $\lambda = 0.0001, 0.001, 0.01, 0.1, 1$. We evaluate the number of iterations according to the relation between the SNR and iteration number, and the number of iteration which leads to the highest SNR is the

$$\begin{cases} \left(\left({}_{a_1}D_x^{\alpha(x,y)}\right)^* \frac{a_1 D_x^{\alpha(x,y)} u^n}{|\nabla^{\alpha(x,y)} u^n|}\right)_{i,j} = \left({}_{x}D_{b_1}^{\alpha(x,y)} \frac{a_1 D_x^{\alpha(x,y)} u^n}{|\nabla^{\alpha(x,y)} u^n|}\right)_{i,j}, \\ \left(\left({}_{a_2}D_y^{\alpha(x,y)}\right)^* \frac{a_2 D_y^{\alpha(x,y)} u^n}{|\nabla^{\alpha(x,y)} u^n|}\right)_{i,j} = \left({}_{y}D_{b_2}^{\alpha(x,y)} \frac{a_2 D_y^{\alpha(x,y)} u^n}{|\nabla^{\alpha(x,y)} u^n|}\right)_{i,j}, \end{cases} \tag{26}$$

$$\begin{cases} \left(\left({}_{a_1}D_x^{\alpha(x,y)}\right)^* \frac{a_1 D_x^{\alpha(x,y)} u^n}{|\nabla^{\alpha(x,y)} u^n|}\right)_{i,j} = \sum_{k=0}^{N-i} (-1)^k \binom{\alpha_{i+k,j}}{k} \left(\frac{a_1 D_x^{\alpha(x,y)} u^n}{|\nabla^{\alpha(x,y)} u^n|}\right)_{i+k,j}, \\ \left(\left({}_{a_2}D_y^{\alpha(x,y)}\right)^* \frac{a_2 D_y^{\alpha(x,y)} u^n}{|\nabla^{\alpha(x,y)} u^n|}\right)_{i,j} = \sum_{k=0}^{N-j} (-1)^k \binom{\alpha_{i,j+k}}{k} \left(\frac{a_2 D_y^{\alpha(x,y)} u^n}{|\nabla^{\alpha(x,y)} u^n|}\right)_{i,j+k}, \end{cases} \quad \text{for} i,\ j = 1, 2, \ldots, N. \tag{27}$$

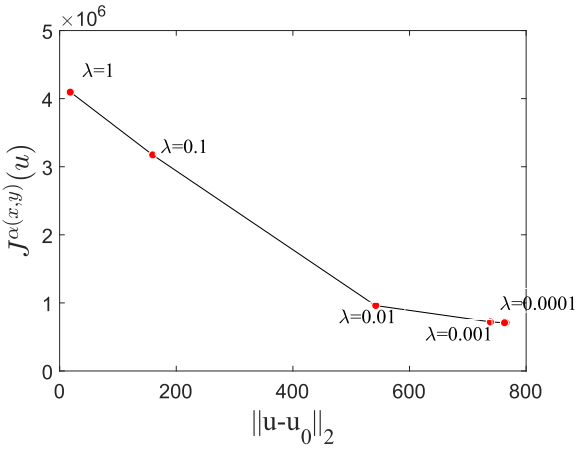

FIGURE 2. L curve for problem (12).

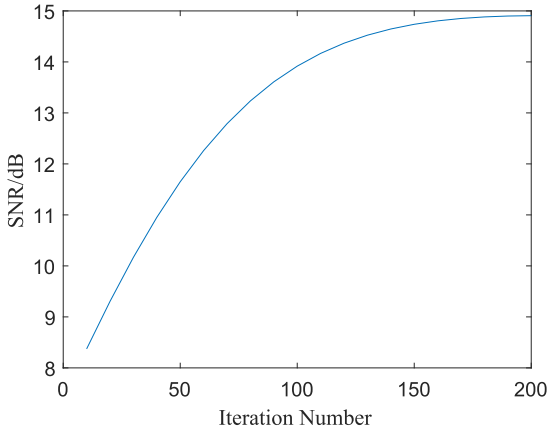

FIGURE 3. Curve for the SNR versus iteration number.

optimal selection. As shown in Figure 3, the optimal iteration number is set as $K = 200$. The other parameters involved in this test are set as $k = 0.05$, $\Delta t = 0.1$. More details about the selection of the parameters involved in the other contrastive methods are referred to the related [14], [28], [32], [33] and [49].

In this test, we show the denoising results in the case of the noise standard deviation $\sigma = 20$ shown in Figure 4(c)-4(h). As seen from the denoised results of the white rectangular region I, our method can effectively alleviate the staircase effect and preserve its structural information while effectively remove the noise in the smooth regions of the noisy image. As seen from the denoised results of the red rectangular region II, our method can effectively preserve edge information while improving the total image quality. For example, TV model can preserve the edges but its denoising effect is not satisfied; the two models of LLT and TGV^2_α-L^2 can get a cleaner image but they cause excessive smoothing on the edges and fail to preserve the structure information well; the edge-preserving ability of FTV model and the improvement of SNR of FTV and SODTGV are not as good as those of our proposed method.

Figure 6 presents the denoised results of these noisy images in Figure 5 to further verify the effectiveness of the proposed method compared with the related state-of-the-art methods like TV, LLT, TGV, FTV and SODTGV. As seen from the first column, our proposed method can get a better visual effect than the other related methods. As seen from the rectangular regions in the second column, our proposed method is superior to the LLT model, the TGV model and the FTV model in preserving edge information. Compared with the TV and SODTGV methods, our method achieves a higher SNR of the denoised image. It can be seen from the lower left rectangular areas which are the enlarged areas of the local images with the same degree in the third column, our method can preserve more image details than the other related methods.

Table 1-Table 3 show the performance of noise removal and the structural similarity in different noise standard deviations $\sigma = 10$, $\sigma = 20$, and $\sigma = 30$ by comparing the proposed method with the TV, LLT, TGV, FTV, and SODTGV methods. It can be seen from these tables, by appropriately tuning the involved parameters, our proposed method can achieve a better trade-off between the improvement of SNR and the preservation of structural similarity (SSIM) compared with the other methods. Here, the two error metrics such as SNR [30] and SSIM [50] are employed to quantitatively verify the effectiveness of the proposed method.

B. REAL SEISMIC DATA EXPERIMENTS

In this subsection, we employ a two-dimensional post-stack seismic data shown in Figure 7(a), and compare with other contrastive methods to verify the denoising effect of our proposed method shown in Figure 7(b)-7(g). Obviously, the 2D field data suffers from heavy random noise which goes against follow-up seismic data interpretation. It is well known for the attributes of seismic data that both lateral continuity of seismic events and the vertical resolution of seismic profiles have important geological significance, in which the lateral continuity of seismic events can be used to interpret the continuity of the stratum in the horizontal direction and a clear stratum structure can be seen from the vertical resolution of seismic profiles.

We compare the denoising effects provided by different methods from the two aspects such as the lateral continuity of seismic reflection events and the vertical resolution of seismic profiles. In practical problems, the noise variance is commonly unknown, we recommend that one can firstly estimate the noise variance by the existing method [51], and then one can set the parameters by the corresponding schemes introduced in above synthetic data example. For simplicity, in this paper, we choose the values of the parameters by hand which can give the satisfactory experimental results. We set the parameters involved in this test as $\lambda = 0.08$, $K = 100$, $k = 0.05$, $\Delta t = 0.1$ which leads to the satisfactory

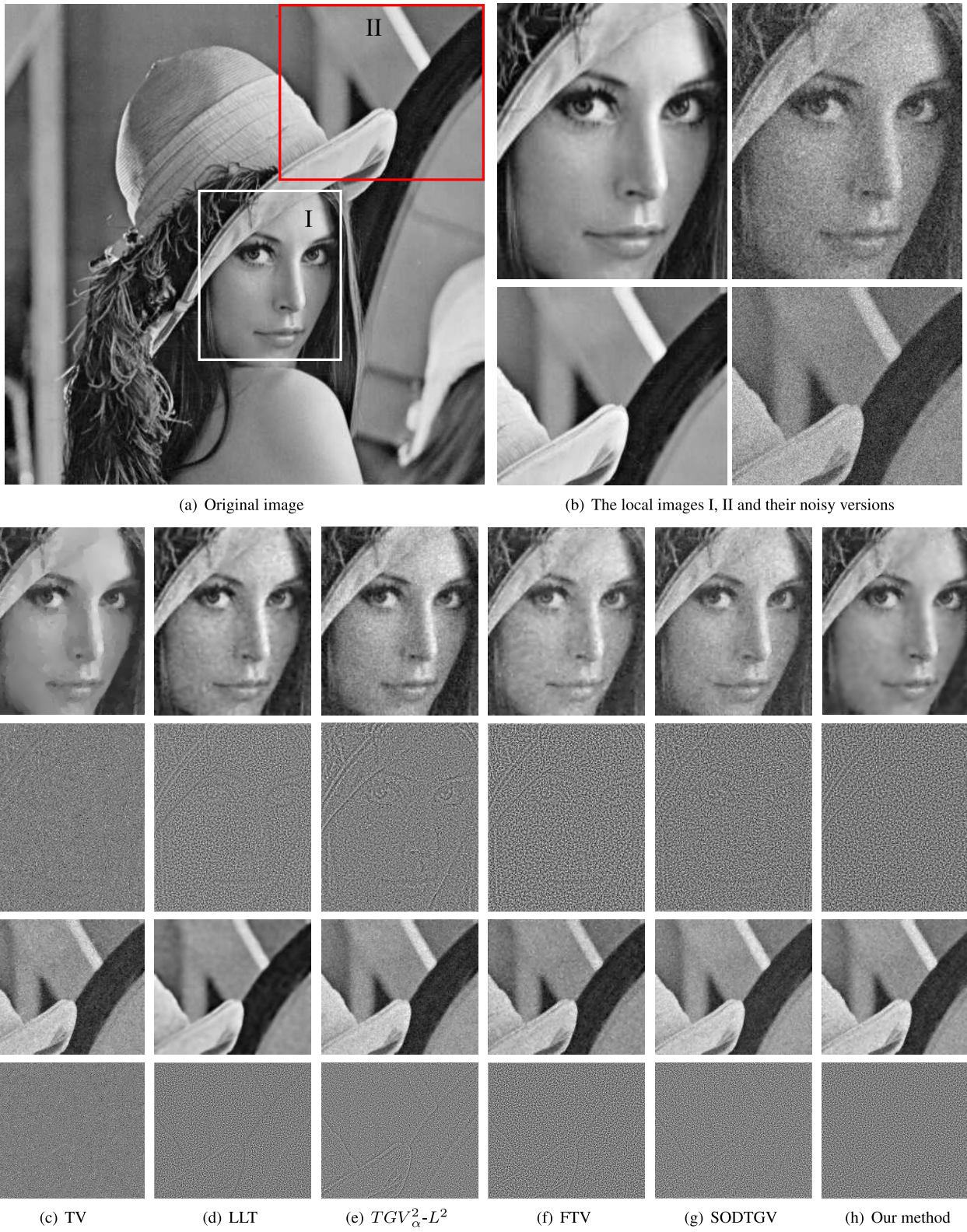

(a) Original image (b) The local images I, II and their noisy versions

(c) TV (d) LLT (e) TGV^2_α-L^2 (f) FTV (g) SODTGV (h) Our method

FIGURE 4. A comparison of the denoising results of the local images by different methods.

experimental results. The parameters involved in the other contrastive methods are set the same as the counterparts of the synthetic image experiments. As shown in the regions from 0.5 s to 1 s in the denoised seismic profiles, the proposed method can enhance the lateral continuity of seismic events more clearly than the other methods. The strong and weak

(a) Test image III and its noisy version

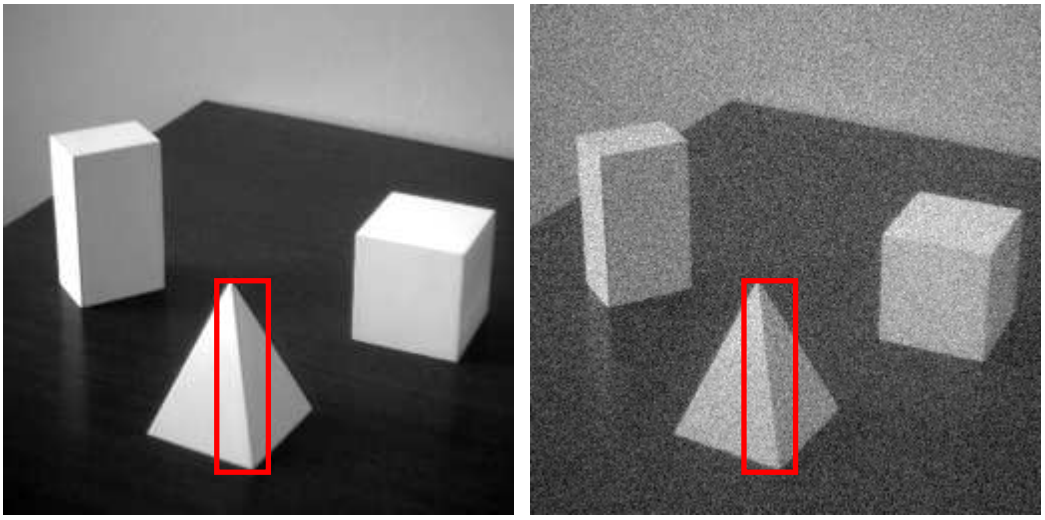

(b) Test image IV and its noisy version

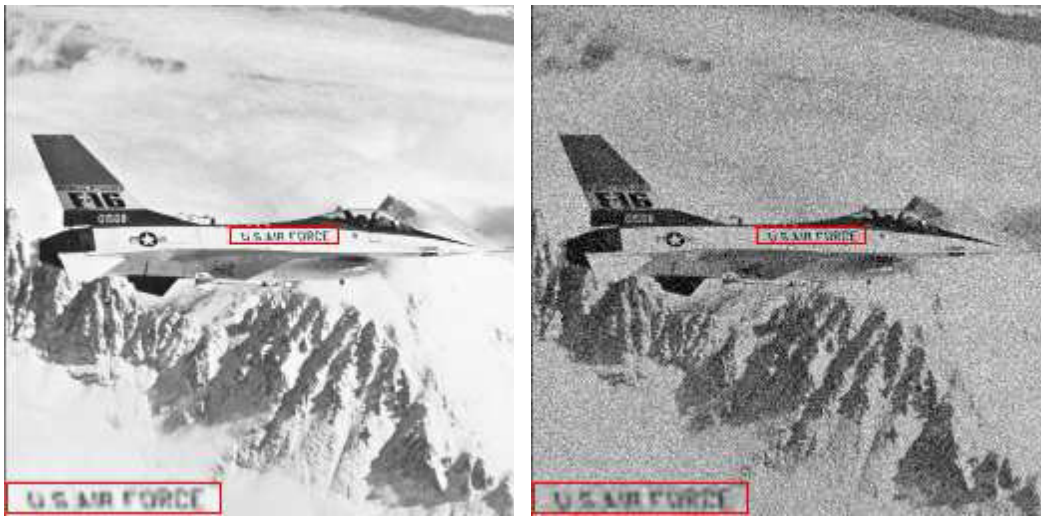

(c) Test image V and its noisy version

FIGURE 5. **Some original test images and their noisy versions.**

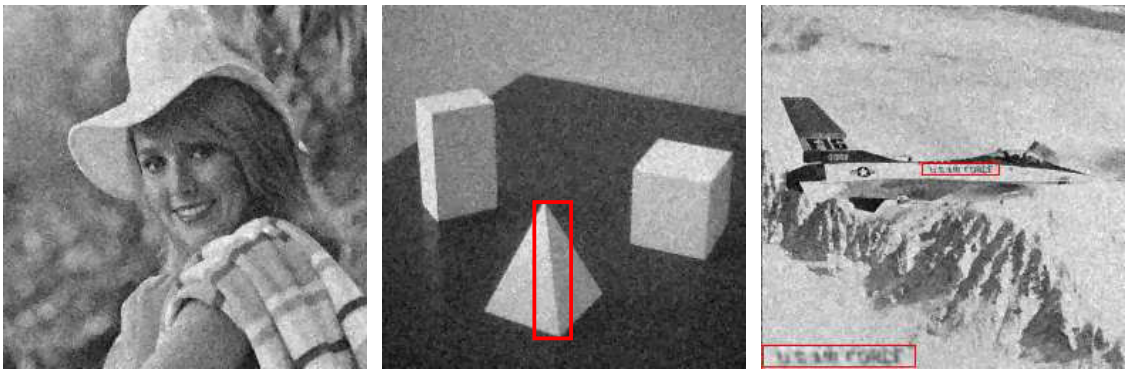

(a) The denoising results by the TV model

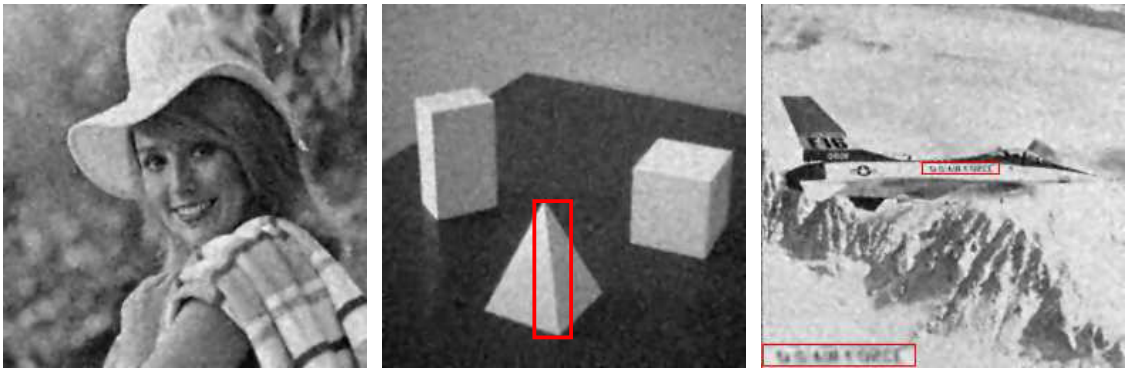

(b) The denoising results by the LLT model

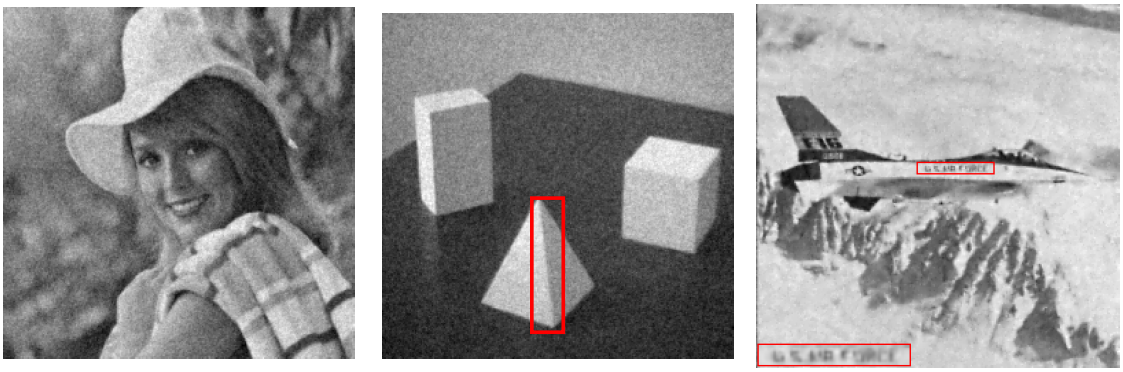

(c) The denoising results by the TGV^2_α-L^2 model

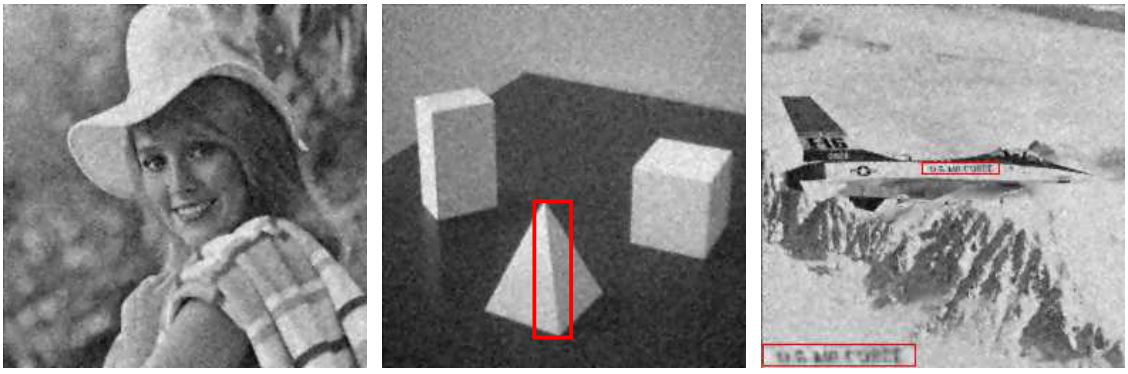

(d) The denoising results by the FTV model

FIGURE 6. **The denoising results by different methods for the test images III-V.**

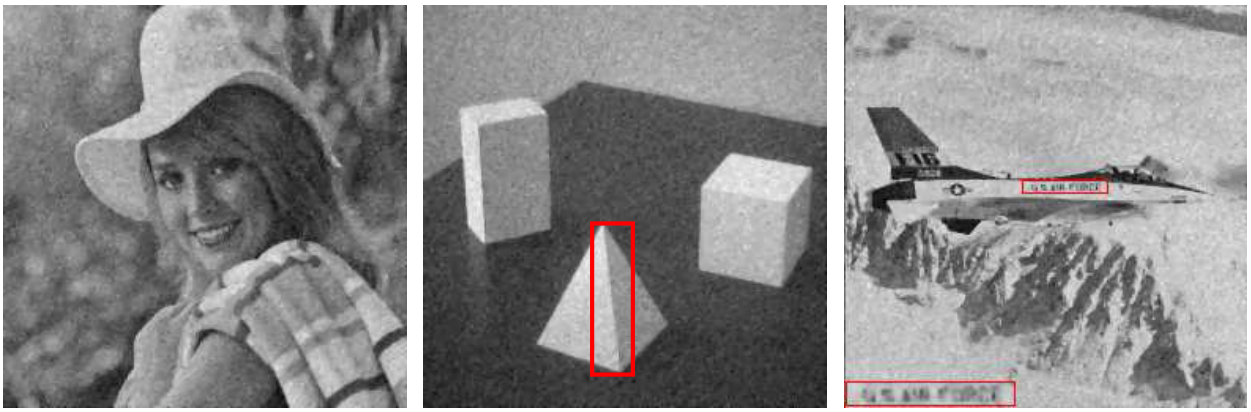

(e) The denoising results by the SODTGV model

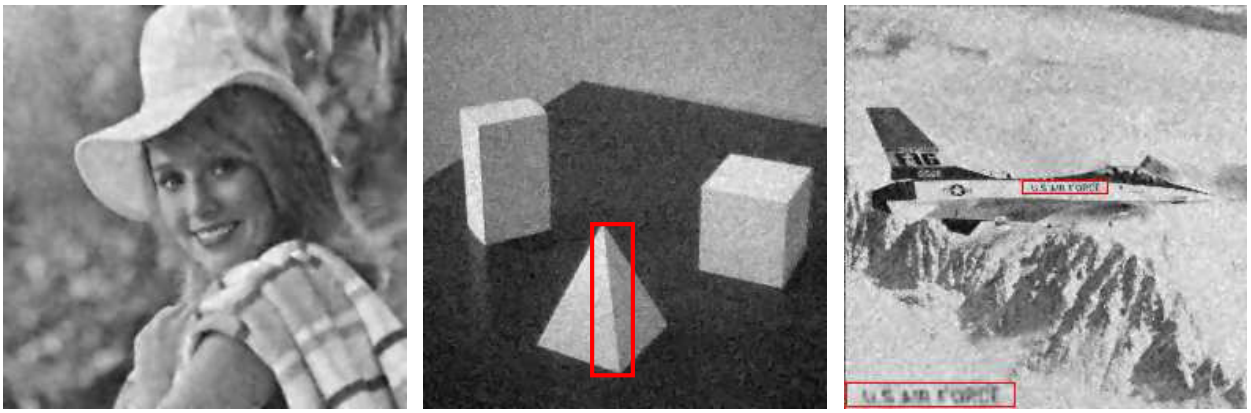

(f) The denoising results by the proposed method

FIGURE 6. ***(Continued.)*** **The denoising results by different methods for the test images III-V.**

TABLE 1. **A comparison of denoising results of the noisy images with the standard deviation of 10.**

		TV		LLT		TGV^2_α-L^2		FTV		SODTGV		Our method	
Image	SNR_0	SNR	SSIM	SNR	SSIM	SNR	SSIM	SNR	SSIM	SNR	SSIM	SNR	SSIM
I	14.01	17.72	0.83	18.57	0.89	18.14	0.85	18.16	0.90	19.14	0.91	**19.21**	**0.91**
II	14.38	19.10	0.78	22.21	0.90	19.93	0.81	21.18	0.90	21.12	0.90	**21.98**	**0.93**
III	13.25	16.26	0.82	16.69	0.79	15.64	0.84	15.80	0.82	16.24	0.83	**16.62**	**0.85**
IV	15.28	20.69	0.78	25.59	0.94	21.98	0.79	24.26	0.95	24.31	0.93	**25.08**	**0.95**
V	13.06	15.33	0.83	16.44	0.88	15.90	0.83	16.08	0.91	16.15	0.90	**16.35**	**0.91**

TABLE 2. **A comparison of denoising results of the noisy images with the standard deviation of 20.**

		TV		LLT		TGV^2_α-L^2		FTV		SODTGV		Our method	
Image	SNR_0	SNR	SSIM	SNR	SSIM	SNR	SSIM	SNR	SSIM	SNR	SSIM	SNR	SSIM
I	7.94	12.62	0.48	14.59	0.62	13.67	0.51	13.35	0.59	14.39	0.70	**14.46**	**0.71**
II	8.36	12.46	0.42	16.33	0.28	14.46	0.31	14.96	0.36	15.76	0.49	**15.97**	**0.51**
III	7.24	11.73	0.54	14.09	0.59	12.62	0.57	13.31	0.59	13.21	0.65	**13.77**	**0.65**
IV	9.27	14.70	0.19	19.25	0.24	15.46	0.17	17.16	0.22	18.12	0.34	**18.65**	**0.36**
V	7.07	11.27	0.45	13.99	0.53	13.01	0.52	12.79	0.50	12.85	0.60	**13.05**	**0.61**

contrast of seismic events shown in above regions tells us that our method provides a higher vertical resolution than the TV, LLT, TGV and FTV based methods. Specifically, the stair-case effects always exist in the denoised results computed by the TV, TGV and FTV based methods, the vertical resolution of the denoised result computed by the LLT based method is lower than the proposed method, and the SODTGV based method leads to some more damages to the seismic reflection events in the regions from 0.5 s to 1 s in the denoised seismic profile.

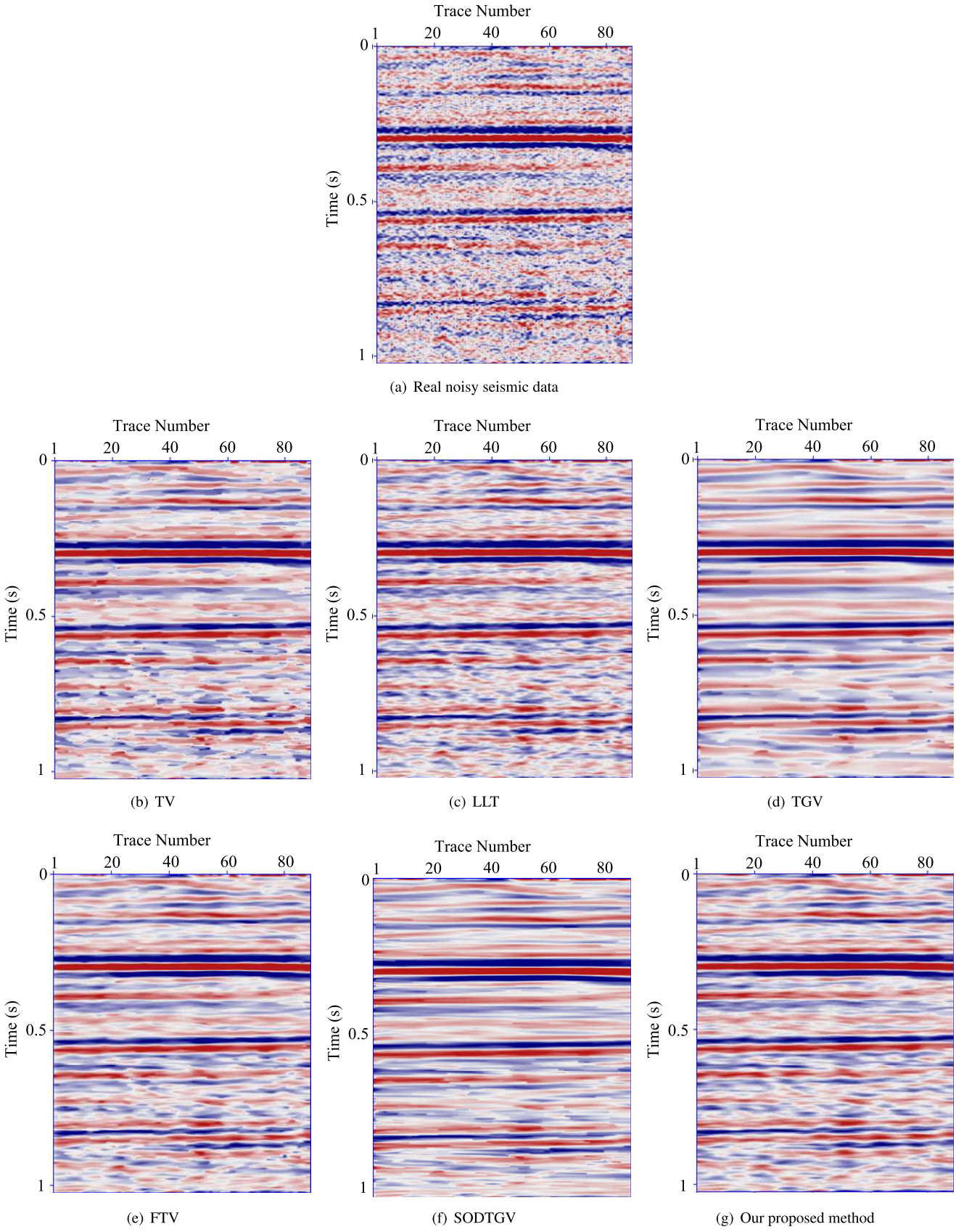

(a) Real noisy seismic data

(b) TV

(c) LLT

(d) TGV

(e) FTV

(f) SODTGV

(g) Our proposed method

FIGURE 7. A comparison of the denoising results for the real seismic data by using different methods.

TABLE 3. A comparison of denoising results of the noisy images with the standard deviation of 30.

		TV		LLT		TGV^2_α-L^2		FTV		SODTGV		Our method	
Image	SNR_0	SNR	SSIM	SNR	SSIM	SNR	SSIM	SNR	SSIM	SNR	SSIM	SNR	SSIM
I	4.38	6.67	0.34	11.64	0.59	10.65	0.52	8.63	0.43	11.06	0.56	**11.59**	**0.61**
II	4.84	7.26	0.25	12.30	0.49	11.31	0.41	9.18	0.32	12.16	0.35	**12.24**	**0.51**
III	3.72	5.99	0.39	10.42	0.59	9.77	0.54	7.80	0.46	9.41	0.49	**9.84**	**0.67**
IV	5.72	8.14	0.21	13.37	0.45	12.27	0.36	10.10	0.28	12.68	0.41	**13.30**	**0.46**
V	3.55	5.73	0.39	9.82	0.58	9.12	0.51	7.43	0.45	9.14	0.58	**9.51**	**0.63**

Therefore, we can conclude that the proposed method has a outstanding performance in enhancing the lateral continuity of seismic events and improving the vertical resolution of seismic profiles while attenuating the random noise.

VI. CONCLUSION

In this paper, we introduced an edge detection function based on the Gaussian filtering operator, established the spatially adaptive fractional edge-preserving denoising model in the variational framework, and discussed the existence and uniqueness of the solution of the proposed model. This proposed model generalizes the TV model and the LLT model. In the experiment part, we applied the proposed method to the synthetic images and real seismic data denoising to verify the effectiveness of our method and compared the experimental results of our method with the related state-of-the-art methods. Experimental results illustrate that our proposed method can not only improve the SNR but also adaptively preserve the structural information of an image. For example, it can be seen from Table 1-Table 3, our proposed method can achieve a better trade-off between the improvement of SNR and the preservation of structural similarity compared with the other methods. This work can provide a new approach for solving the ill-posed inverse problems in engineering science.

REFERENCES

[1] J. Weickert, *Anisotropic Diffusion in Image Processing*, vol. 1. Stuttgart, Germany: Teubner, 1998.

[2] T. F. Chan, J. Shen, and L. Vese, "Variational PDE models in image processing," *Notices AMS*, vol. 50, no. 1, pp. 14–26, 2003.

[3] S. Bettahar, P. Lambert, and A. B. Stambouli, "PDE-based efficient method for colour image restoration," *Comput. Math. Appl.*, vol. 74, no. 3, pp. 577–590, Aug. 2017.

[4] X. Li, H. Shen, L. Zhang, H. Zhang, Q. Yuan, and G. Yang, "Recovering quantitative remote sensing products contaminated by thick clouds and shadows using multitemporal dictionary learning," *IEEE Trans. Geosci. Remote Sens.*, vol. 52, no. 11, pp. 7086–7098, Nov. 2014.

[5] M. Elad and M. Aharon, "Image denoising via learned dictionaries and sparse representation," in *Proc. IEEE Comput. Soc. Conf. Comput. Vis. Pattern Recognit. (CVPR)*, vol. 1, Jun. 2006, pp. 895–900.

[6] A. Kumar, M. O. Ahmad, and M. N. S. Swamy, "A framework for image denoising using first and second order fractional overlapping group sparsity (HF-OLGS) regularizer," *IEEE Access*, vol. 7, pp. 26200–26217, 2019.

[7] J. Liu and S. Osher, "Block matching local SVD operator based sparsity and TV regularization for image denoising," *J. Sci. Comput.*, vol. 78, no. 1, pp. 1–18, 2019.

[8] X. Li, L. Wang, Q. Cheng, P. Wu, W. Gan, and L. Fang, "Cloud removal in remote sensing images using nonnegative matrix factorization and error correction," *ISPRS J. Photogramm. Remote Sens.*, vol. 148, pp. 103–113, Feb. 2019.

[9] P. Perona and J. Malik, "Scale-space and edge detection using anisotropic diffusion," *IEEE Trans. Pattern Anal. Mach. Intell.*, vol. 12, no. 7, pp. 629–639, Jul. 1990.

[10] J. Bai and X.-C. Feng, "Fractional-order anisotropic diffusion for image denoising," *IEEE Trans. Image Process.*, vol. 16, no. 10, pp. 2492–2502, Oct. 2007.

[11] P. Guidotti and J. V. Lambers, "Two new nonlinear nonlocal diffusions for noise reduction," *J. Math. Imag. Vis.*, vol. 33, no. 1, pp. 25–37, Jan. 2009.

[12] M. Janev, S. Pilipović, T. Atanacković, R. Obradović, and N. Ralević, "Fully fractional anisotropic diffusion for image denoising," *Math. Comput. Model.*, vol. 54, nos. 1–2, pp. 729–741, Jul. 2011.

[13] Q. Zhou, J. Gao, Z. Wang, and K. Li, "Adaptive variable time fractional anisotropic diffusion filtering for seismic data noise attenuation," *IEEE Trans. Geosci. Remote Sens.*, vol. 54, no. 4, pp. 1905–1917, Apr. 2016.

[14] L. I. Rudin, S. Osher, and E. Fatemi, "Nonlinear total variation based noise removal algorithms," *Phys. D, Nonlinear Phenomena*, vol. 60, nos. 1–4, pp. 259–268, 1992.

[15] G. Gilboa, N. Sochen, and Y. Y. Zeevi, "Variational denoising of partly textured images by spatially varying constraints," *IEEE Trans. Image Process.*, vol. 15, no. 8, pp. 2281–2289, Aug. 2006.

[16] X. Liu, L. Huang, and Z. Guo, "Adaptive fourth-order partial differential equation filter for image denoising," *Appl. Math. Lett.*, vol. 24, no. 8, pp. 1282–1288, Aug. 2011.

[17] X.-L. Zhao, W. Wang, T.-Y. Zeng, T.-Z. Huang, and M. K. Ng, "Total variation structured total least squares method for image restoration," *SIAM J. Sci. Comput.*, vol. 35, no. 6, pp. B1304–B1320, Jan. 2013.

[18] X.-L. Zhao, F. Wang, and M. K. Ng, "A new convex optimization model for multiplicative noise and blur removal," *SIAM J. Imag. Sci.*, vol. 7, no. 1, pp. 456–475, Jan. 2014.

[19] S. Wang, T.-Z. Huang, X.-L. Zhao, J.-J. Mei, and J. Huang, "Speckle noise removal in ultrasound images by first-and second-order total variation," *Numer. Algorithms*, vol. 78, no. 2, pp. 513–533, Jun. 2018.

[20] M.-G. Shama, T.-Z. Huang, J. Liu, and S. Wang, "A convex total generalized variation regularized model for multiplicative noise and blur removal," *Appl. Math. Comput.*, vol. 276, pp. 109–121, Mar. 2016.

[21] I. Uddin, J. Ali, and J. J. Nieto, "An iteration scheme for a family of multivalued mappings in CAT(0) spaces with an application to image recovery," *Revista de la Real Academia de Ciencias Exactas, Físicas y Naturales. Serie A. Matemáticas*, vol. 112, no. 2, pp. 373–384, Apr. 2018.

[22] D. N. H. Thanh, L. T. Thanh, N. N. Hien, and S. Prasath, "Adaptive total variation L1 regularization for salt and pepper image denoising," *Optik*, vol. 208, Apr. 2020, Art. no. 163677.

[23] S. Esedoḡlu and S. J. Osher, "Decomposition of images by the anisotropic Rudin-Osher-Fatemi model," *Commun. Pure Appl. Math., J. Issued Courant Inst. Math. Sci.*, vol. 57, no. 12, pp. 1609–1626, 2004.

[24] T. F. Chan and X.-C. Tai, "Identification of discontinuous coefficients in elliptic problems using total variation regularization," *SIAM J. Sci. Comput.*, vol. 25, no. 3, pp. 881–904, Jan. 2003.

[25] A. Chambolle and P.-L. Lions, "Image recovery via total variation minimization and related problems," *Numerische Math.*, vol. 76, no. 2, pp. 167–188, Apr. 1997.

[26] T. Chan, A. Marquina, and P. Mulet, "High-order total variation-based image restoration," *SIAM J. Sci. Comput.*, vol. 22, no. 2, pp. 503–516, 2000.

[27] Y.-L. You and M. Kaveh, "Fourth-order partial differential equations for noise removal," *IEEE Trans. Image Process.*, vol. 9, no. 10, pp. 1723–1730, Oct. 2000.

[28] M. Lysaker, A. Lundervold, and X.-C. Tai, "Noise removal using fourth-order partial differential equation with applications to medical magnetic resonance images in space and time," *IEEE Trans. Image Process.*, vol. 12, no. 12, pp. 1579–1590, Dec. 2003.
[29] P. Guidotti and K. Longo, "Two enhanced fourth order diffusion models for image denoising," *J. Math. Imag. Vis.*, vol. 40, no. 2, pp. 188–198, Jun. 2011.
[30] D. Wang and J. Gao, "An improved noise removal model based on nonlinear fourth-order partial differential equations," *Int. J. Comput. Math.*, vol. 93, no. 6, pp. 942–954, Jun. 2016.
[31] M. Lysaker and X.-C. Tai, "Iterative image restoration combining total variation minimization and a second-order functional," *Int. J. Comput. Vis.*, vol. 66, no. 1, pp. 5–18, Jan. 2006.
[32] K. Bredies, K. Kunisch, and T. Pock, "Total generalized variation," *SIAM J. Imag. Sci.*, vol. 3, no. 3, pp. 492–526, 2010.
[33] J. Zhang and Z. Wei, "Fractional variational model and algorithm for image denoising," in *Proc. 4th Int. Conf. Natural Comput.*, vol. 5, 2008, pp. 524–528.
[34] Z. Jun and W. Zhihui, "A class of fractional-order multi-scale variational models and alternating projection algorithm for image denoising," *Appl. Math. Model.*, vol. 35, no. 5, pp. 2516–2528, May 2011.
[35] J. Zhang and K. Chen, "A total fractional-order variation model for image restoration with nonhomogeneous boundary conditions and its numerical solution," *SIAM J. Imag. Sci.*, vol. 8, no. 4, pp. 2487–2518, Jan. 2015.
[36] D. Chen, Y. Chen, and D. Xue, "Fractional-order total variation image denoising based on proximity algorithm," *Appl. Math. Comput.*, vol. 257, pp. 537–545, Apr. 2015.
[37] A. Ullah, W. Chen, and M. A. Khan, "A new variational approach for restoring images with multiplicative noise," *Comput. Math. with Appl.*, vol. 71, no. 10, pp. 2034–2050, May 2016.
[38] G. Chen, J. Zhang, D. Li, and H. Chen, "Robust Kronecker product video denoising based on fractional-order total variation model," *Signal Process.*, vol. 119, pp. 1–20, Feb. 2016.
[39] D. Li, X. Tian, Q. Jin, and K. Hirasawa, "Adaptive fractional-order total variation image restoration with split Bregman iteration," *ISA Trans.*, vol. 82, pp. 210–222, Nov. 2018.
[40] W. Wang, X.-G. Xia, S. Zhang, C. He, and L. Chen, "Vector total fractional-order variation and its applications for color image denoising and decomposition," *Appl. Math. Model.*, vol. 72, pp. 155–175, Aug. 2019.
[41] M. R. Chowdhury, J. Zhang, J. Qin, and Y. Lou, "Poisson image denoising based on fractional-order total variation," *Inverse Problems Imag.*, vol. 14, no. 1, p. 77, 2020.
[42] D. Wang and J. Gao, "A new method for random noise attenuation in seismic data based on anisotropic fractional-gradient operators," *J. Appl. Geophys.*, vol. 110, pp. 135–143, Nov. 2014.
[43] F. Catté, P.-L. Lions, J.-M. Morel, and T. Coll, "Image selective smoothing and edge detection by nonlinear diffusion," *SIAM J. Numer. Anal.*, vol. 29, no. 1, pp. 182–193, Feb. 1992.
[44] Z. Guo, J. Sun, D. Zhang, and B. Wu, "Adaptive Perona–Malik model based on the variable exponent for image denoising," *IEEE Trans. Image Process.*, vol. 21, no. 3, pp. 958–967, Mar. 2012.
[45] Y.-F. Pu, J.-L. Zhou, and X. Yuan, "Fractional differential mask: A fractional differential-based approach for multiscale texture enhancement," *IEEE Trans. Image Process.*, vol. 19, no. 2, pp. 491–511, Feb. 2010.
[46] D. Valério and J. Sá da Costa, "Variable-order fractional derivatives and their numerical approximations," *Signal Process.*, vol. 91, no. 3, pp. 470–483, Mar. 2011.
[47] N. L. Carothers, *Real Analysis*. Cambridge, U.K.: Cambridge Univ. Press, 2000.
[48] G. Aubert and J.-F. Aujol, "A variational approach to removing multiplicative noise," *SIAM J. Appl. Math.*, vol. 68, no. 4, pp. 925–946, Jan. 2008.
[49] D. Wang, J. Gao, N. Liu, and X. Jiang, "Structure-oriented DTGV regularization for random noise attenuation in seismic data," *IEEE Trans. Geosci. Remote Sens.*, early access, Jun. 19, 2020, doi: 10.1109/TGRS.2020.3001141.
[50] Z. Wang, A. C. Bovik, H. R. Sheikh, and E. P. Simoncelli, "Image quality assessment: From error visibility to structural similarity," *IEEE Trans. Image Process.*, vol. 13, no. 4, pp. 600–612, Apr. 2004.
[51] G. Liu, S. Fomel, L. Jin, and X. Chen, "Stacking seismic data using local correlation," *Geophysics*, vol. 74, no. 3, pp. V43–V48, May 2009.

DEHUA WANG received the Ph.D. degree from the School of Information and Communications Engineering, Xi'an Jiaotong University, Xi'an, Shaanxi, China, in 2016. Since 2016, he has been working with the School of Science, Xi'an Technological University, Xi'an. He is currently engaged in a postdoctoral research position with the School of Mathematical Sciences, University of Electronic Science and Technology of China, Chengdu, Sichuan, China. His research interests include machine learning, seismic data processing, the mathematical modeling, and optimization algorithms for seismic inversion problems.

JUAN J. NIETO, photograph and biography not available at the time of publication.

XIAOPING LI received the B.S. degree in mathematics from Sichuan Normal University, in 2006, and the Ph.D. degree in information and communication engineering from Xi'an Jiaotong University, in 2016. From 2006 to 2010, he was an Assistant Professor with the College of Information Engineering, Tarim University, Alar, China. From December 2013 to January 2015, he was a Visiting Scholar with the Department of Electrical and Computer Engineering, University of Delaware, Newark. He is currently an Associate Professor with the University of Electronic Science and Technology of China. His main research interests include signal processing theory, computer cryptography, and coding theory.

YIMING LI is currently pursuing the bachelor's degree with the Department of Mathematical Sciences, Fudan University. His research interests include computational mathematics, especially in numerical optimization algorithms for differential equations. He is also good at the skills in software, such as R, MATLAB, python, SPSS, Latex, and so on.